Design and Vibratory Loads Reduction Analysis of Advanced Active Twist Rotor Blades Incorporating Single Crystal Piezoelectric Fiber Composites

Jae-Sang Park*
Department of Aerospace Information Engineering,
Konkuk University, Seoul 143-701, Korea

Sang-Joon Shin**
School of Mechanical and Aerospace Engineering,
Seoul National University, Seoul 151-742, Korea

Deog-Kwan Kim***
Korea Aerospace Research Institute,
Daejeon 305-333, Korea

Abstract

This paper presents design optimization of a new Active Twist Rotor (ATR) blade and conducts its aeroelastic analysis in forward flight condition. In order to improve a twist actuation performance, the present ATR blade utilizes a single crystal piezoelectric fiber composite actuator and the blade cross-sectional layout is designed through an optimization procedure. The single crystal piezoelectric fiber composite actuator has excellent piezoelectric strain performance when compared with the previous piezoelectric fiber composites such as Active Fiber Composites (AFC) and Macro Fiber Composites (MFC). Further design optimization gives a cross-sectional layout that maximizes the static twist actuation while satisfying various blade design requirements. After the design optimization is completed successfully, an aeroelastic analysis of the present ATR blade in forward flight is conducted to confirm the efficiency in reducing the vibratory loads at both fixed- and rotating-systems. Numerical simulation shows that the present ATR blade utilizing single crystal piezoelectric fiber composites may reduce the vibratory loads significantly even with much lower input-voltage when compared with that used in the previous ATR blade. However, for an application of the present single crystal piezoelectric actuator to a full scaled rotor blade, several issues exist. Difficulty of manufacturing in a large size and severe brittleness in its material characteristics will need to be examined.

Key Words : Active Twist Rotor blades, Single crystal piezoelectric fiber composites, Design optimization, Aeroelastic Analysis

Introduction

High vibratory load induced in the forward flight is one of the most serious problems in rotorcrafts. Such high vibratory load makes serious constraints such as a relatively poor ride quality, a restricted flight envelope, low fatigue life in the structural components, and a resulting high operating cost. The primary reason of high vibration level is the complex unsteady aerodynamic condition including asymmetry of the rotor disk aerodynamics, blade-

* Research Professor
E-mail : smartrotor@gmail.com Tel : 02-458-1901 Fax : 02-444-6670
** Professor
** Korea Aerospace Research Institute

vortex interaction, retreating blade-stall, high advancing blade Mach numbers and low aerodynamic lag damping.

In order to alleviate this problem, active rotor control methodologies, which are to modify directly the periodic aerodynamic loads acting upon the rotor blades, have been examined during the last few decades. These may be broadly classified as Higher Harmonic Control (HHC, [1]) and Individual Blade Control (IBC, [2]). HHC was introduced in the 1970s and has shown to reduce vibration and noise by implementing active control of the rotor swashplate to change the pitch at the root of the blades. IBC typically uses hydraulically-actuated pitch links to achieve active control of each blade independently. Although both HHC and IBC showed several outstanding results for both a wind-tunnel model [1-3] and a flight test [4], some difficulties still existed in providing the required hydraulic power in the rotating system. Other constraints also showed up, such as an adverse power requirement and a limitation on excitation frequency in the case of HHC, and extreme mechanical complexity of the hydraulic sliprings in the case of IBC.

Since 1990s, various active rotor control methods based on the piezoelectric actuators, such as Active Trailing-edge Flaps (ATF, Figure 1(a)) and Active Twist Rotor (ATR, Figure 1(b)), have been suggested. The ATR blade utilizes piezoelectric fiber composite actuators such as AFC [5] or MFC [6], that are embedded directly within the composite blade skin. These actuators produce strain-induced twisting deformations in the blade, when activated by an electrical voltage. Under the NASA/Army/MIT ATR program until 2003, the ATR blade using AFC was designed, manufactured and tested successfully. An ATR prototype blade was designed and fabricated for bench and hover tests [7, 8]. After minor design modification, a set of ATR blades were manufactured, analyzed and wind-tunnel-tested in a forward flight condition [9-10]. As a result, during the open-loop forward flight test, significant vibration reduction on both fixed- and rotating-system loads was observed. Finally, a closed-loop controller was designed to reduce the ATR hub shear vibratory loads and implemented successfully in the NASA Langley wind tunnel experimental setup [11].

Following the completion of the ATR Phase-I program, the U.S. Army Research Laboratory Vehicle Technology Directorate began examination on the Advanced ATR (AATR) blade [12] using MFC. The original ATR blade was designed to have a rectangular blade planform and a simple NACA 0012 airfoil. However, the AATR blade incorporated a high performance airfoil and advanced blade tip shape. The AATR blade was designed based on the configuration of a High-Lift Rotor (HLR) concept developed in the U.S. Army Aviation and Missile Command, but still with the characteristics similar to that of the original ATR blade. Another ATR research effort was originated from the EU-sponsored Friendcopter project for an environmentally friendly helicopter, and in which a scaled ATR blade using MFC was developed [13-14]. The EU-ATR blade was based on a passive BO-105 helicopter rotor blade.

Although the previous ATR blades utilizing either AFC or MFC could reduce vibratory loads and acoustic noise of helicopters significantly, a quite high input-voltage up to 2,000 V_{pp} (peak-to-peak voltage) was required. When compared with the ATF technology, such a high input-voltage to obtain the high level of twist actuation authority is a serious obstacle in application of the ATR methodology to the full-scale rotorcraft system.

To solve such drawback in the previous ATR blades, this paper proposes a new AATR (AATR-II) blade which has an improved twist actuation performance. The present improvement of twisting authority makes it possible that the AATR-II blade can reduce the vibratory loads both at fixed- and rotating-system in helicopters in forward flight remarkably even with a much lower input-voltage.

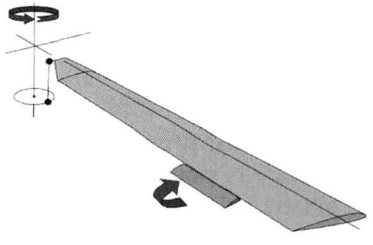

Fig. 1.(a) Active Trailing-edge Flap (ATF) blade

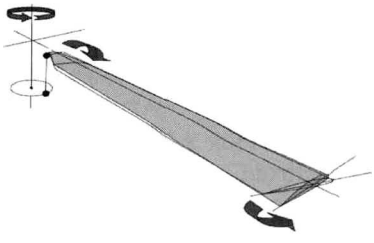

Fig. 1.(b) Active Twist Rotor (ATR) blade

For an improvement of the twist actuation performance, two design aspects are considered as follows in this paper. The first aspect is a use of the single crystal piezoelectric fiber composites instead of the conventional piezoelectric fiber composites such as AFC or MFC. The single crystal piezoelectric fiber composite is a new piezoelectric fiber composite actuator based on a single crystal material [15]. Such single crystal piezoelectric material may produce strain levels more than 1% and exhibit five times larger than that of the conventional piezoceramic material in terms of strain energy density. In addition, it possesses higher coupling coefficients. Although it is still difficult to manufacture the single crystal piezoelectric materials in a large size [16], it will be advantageous to use an improved actuation performance of the piezoelectric fiber composites [16-17]. Therefore, in this paper, the MFC using single crystal PMN-32%PT [18], i.e., the single crystal MFC, is adopted. The second aspect is a systematic design optimization to search for a cross-sectional configuration which produces the maximum tip twist actuation. Since the ATR control technique requires higher twist actuation authority, the blade cross-section needs to be designed so as to maximize the twisting authority. For this reason, the present paper introduces design optimization which finds the cross-section lay-out to maximize the static tip twist actuation. In the case of the ATF blades, there have been reported some research results for a design optimization to minimize the vibration [19-21]. However, a few results [22-23] were found in the literature for a design optimization of the ATR blade and it presents a preliminary establishment of an optimized cross-sectional configuration for an advanced ATR blade. By using such design optimization framework provided by Cesnik and improving it, this paper attempts to determine the cross-section layout of the AATR-II blade which provides the maximum static twist actuation.

After obtaining the optimal cross-sectional configuration, an aeroelastic analysis of the present AATR-II blade in forward flight condition is conducted. In order to predict vibratory loads at both the fixed- and rotating-system in the AATR-II, a nonlinear flexible multibody dynamics code, DYMORE [24], is used. For multi-body dynamic modeling, various rigid bodies, mechanical joints and elastic beams are introduced. Once the steady-state equilibrium condition is obtained, an Individual Blade Control (IBC) mode using sine-dwell signal is applied for the blade control to reduce the vibratory loads. Since ($b+1$, b, $b-1$) frequency components are to influence significantly upon a b-bladed rotor system, only 3, 4 and 5/rev frequency components are considered. Since the present AATR-II blade has an improved twist actuation performance, an advanced performance and efficiency is expected for the present AATR-II system in reducing the vibratory loads in rotorcraft.

Design Optimization Framework of AATR-II Blade

Although the AATR-II blade is a brand new rotor blade, its design is conducted to maintain the characteristics of the original ATR blade based on AFC. Figure 2 and Table 1 show the general configuration and the properties of the original ATR blade, respectively [8]. For a cross-sectional design for the present AATR-II, as shown in Figure 3, the lay-up configuration is basically similar to that of the original ATR blade. In order to maximize the twist actuation, the PMN-32%PT fiber orientation angle of the single crystal MFC is arranged as $\pm 45^\circ$ with respect to the blade spanwise axis. The material properties of E-glass ply [8] and single crystal MFC actuator [17] are summarized in Table 2. Its blade planform is based on that of the AATR blade [12], as shown in Figure 4. It is assumed that the single crystal MFC actuators are distributed from approximately from 29% to 95% blade radius.

In this paper, the design optimization framework developed for the original AATR blade based on the standard MFC [22, 23] is used for the blade design. And, it is improved by updating the version of UM/VABS incorporated in the framework. UM/VABS (University of Michigan/Variational-Asymptotic Beam Cross-Sectional Analysis, [25]) version 1.02 used in the previous AATR optimization computes all the sectional properties at a cross-sectional centroid. On the contrary, the present UM/VABS version 1.23 is capable of estimating the same properties at a shear center, i.e., the elastic axis. This update provides a more accurate estimate for the cross-sectional properties, and then improves the one-dimensional beam analysis result. A basic optimization problem is defined as follows.

Table 1. Properties of the original ATR blade

Rotor type	Fully articulated
Number of blades, b	4
Blade chord, c	0.108 m
Blade radius, R	1.397 m
Solidity, $bc/\pi R$	0.0982
Airfoil section	NACA 0012
Blade linear twist, θ_{tw}	-10°
Hinge offset	0.076 m
Root cutout	0.318 m
Pitch axis	25% chord
Elastic axis	19.6% chord
Center of gravity	23.2% chord
Lock number, γ	9.0
Tip Mach number	0.6
Centrifugal loading at tip	738.5 g
Nominal rotor speed	687.5 RPM
Mass per unit span, m	$0.710 kg/m$
1st torsional frequency at 687.5 RPM	6.97/rev
Twist actuation at 0 RPM and 2,000 V_{pp}	$1.25 \deg/m$

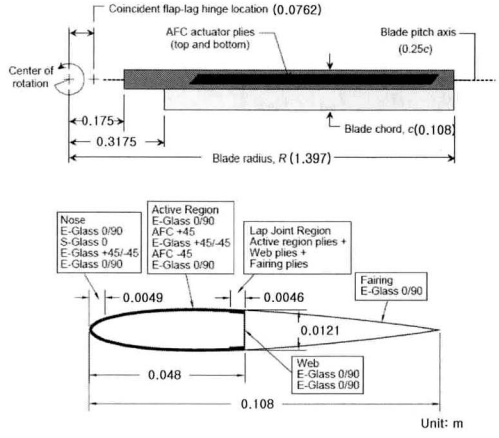

Fig. 2. General configuration of the original ATR blade

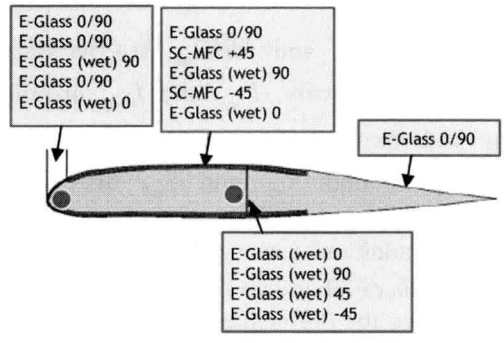

Fig. 3. Layup configuration for the AATR-II blade

maximize $\phi = \phi(\mathbf{x})$

$$\text{maximize } \phi = \phi(\mathbf{x}) \tag{1}$$

where ϕ is an objective function which is the static tip twist actuation due to the the single crystal MFC. As shown in Figure 5, the design variable vector $\mathbf{x}$ is composed of the following parameters.

Table 2. Material properties of an E-glass and standard/single crystal MFCs

Property	E-glass	Standard MFC	Single crystal MFC
E_1 [GPa]	19.3	30.3	6.23
E_2 [GPa]	19.3	15.9	11.08
G_{12} [GPa]	4.1	5.52	2.01
ν_{12}	0.148	0.31	0.23
ρ [kg/m^3]	1700	4480	5338.3
d_{11} [$\times 10^{-12}$ m/V]	0	400	1896.5
d_{12} [$\times 10^{-12}$ m/V]	0	-170	-838.2
Thickness [$\times 10^{-4}$ m]	1.143	3.023	3.023
Electrode spacing [$\times 10^{-4}$ m]	N/A	5.334	5.334

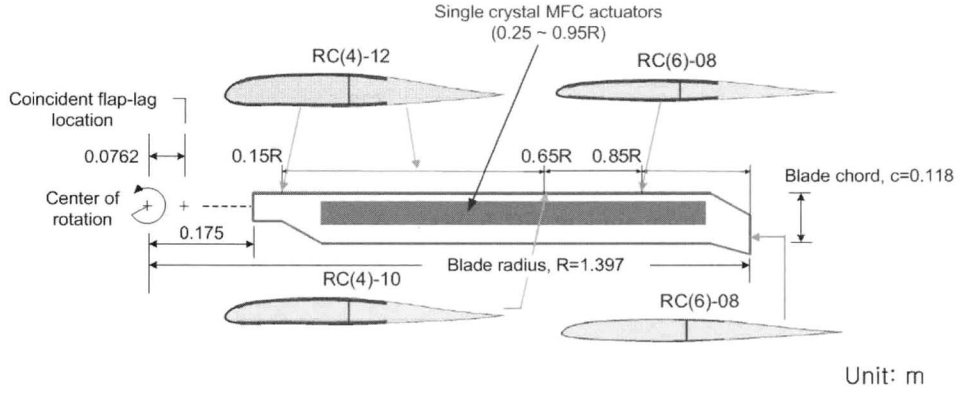

Fig. 4. General configuration of the AATR-II blade

$$\mathbf{x} = \left[MFC_{start} \quad MFC_{end} \quad l_{spar} \quad l_{WebEx} \quad m_1 \quad m_2 \quad l_{m1} \quad l_{m2} \right] \tag{2}$$

where MFC_{start} and MFC_{end} are the starting and ending chordwise-locations of the active region, respectively. l_{spar} and l_{WebEx} are the chordwise-location of the spar and the length of the web extension, respectively. m_1 and m_2 are the masses for two discrete ballast weights. Finally l_{m1} and l_{m2} are their chordwise-locations. In the present design optimization, the thickness and fiber orientation angle of each ply are held as constant.

In addition, various design constraints, $g(\mathbf{x})$, are considered in order to maintain the present blade characteristics as close to those of the original ATR blade. Upper and lower boundaries for the design variable vector $\mathbf{x}$ for the feasible solution are also considered as summarized in Table 3. The constraints for the chordwise locations of the cross-sectional center of gravity, C.G., and the cross-sectional elastic axis, E.A., are taken into account for an aeroelastic stability. The constraints for the blade mass per unit span length and the first torsional frequency of the blade at the nominal rotor speed are accounted in order to match an appropriate Lock number and for a desirable blade dynamics, respectively. Finally, for the structural integrity, the maximum allowable blade local strain constraint under the worst-case loading condition is added. In this paper, since there is not available value for the maximum allowable strain of the single crystal MFC yet, the corresponding value (approximately 6,800 microstrain) for the standard MFC [22, 23] is adopted.

Table 3. Design constraints for design optimization

Property	Constraint
Center of gravity	$0.22c \leq C.G. \leq 0.28c$
Elastic axis	$0.22c \leq E.A. \leq 0.28c$
Blade mass / length	$0.67 \leq m \leq 0.71$
1st torsional frequency at 687.5RPM	$1T \leq 5.0$ /rev
Local strain in the worst loading case	Max. strain < Ultimate strength of the constituent material
Web extension	$0.05c \leq l_{WebEx} \leq 0.25c$
Starting/Ending chordwise-locations of active region	$0.0455c \leq MFC_{start} \leq 0.85c$ $0.0455c \leq MFC_{end} \leq 0.85c$
Spar location	$0.1c \leq l_{spar} \leq 0.85c$

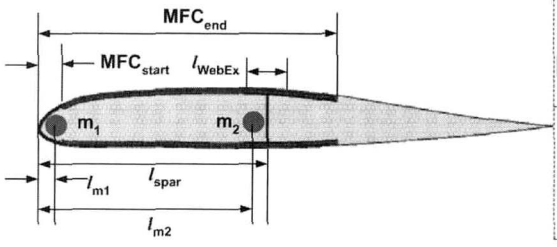

Fig. 5. Design variables for design Optimization

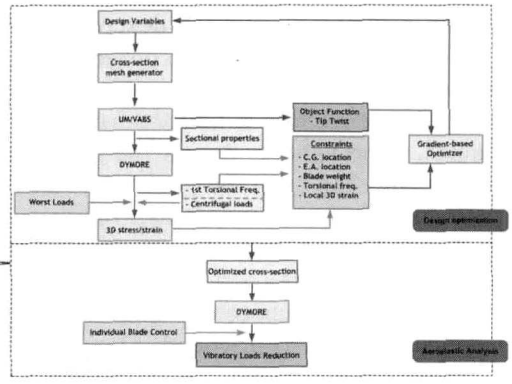

Fig. 6. Design optimization framework for the AATR-II blade

The present design optimization framework consists of various numerical analysis elements as shown in Figure 6. MATLAB provides an environment to integrate all these analysis elements and conducts mathematical optimization. In the present framework, there are three important analysis elements included. First, for the two-dimensional (2-D) linear cross-section analysis, UM/VABS is used. UM/VABS is a finite element based analysis which may calculate the sectional stiffness, inertia matrices and actuation force/moment vectors. In addition, it also determines the chordwise-locations of the center of gravity and the elastic axis. Since UM/VABS is the finite element method, it requires the cross-section mesh generator [26], which takes input parameters and generates the finite element mesh. Second, for the one-dimensional (1-D) nonlinear beam analysis, DYMORE is introduced. The detailed description and capability of DYMORE will be described in a later section regarding the multi-body dynamic modeling of the present AATR-II blade. In the framework, DYMORE uses the sectional properties which are estimated by UM/VABS and calculates the blade natural frequency at the nominal rotor speed. Finally, in order to consider the structural integrity of the blade, the 3-D stress/strain analysis is applied. This element computes an internal local 3-D strain and stress field under the worst-case blade loading. The worst loading condition consists of the sectional blade loads for the flapwise bending, chordwise bending, and torsion which are computed by CAMRAD-II simulation in the previous ATR research and considering centrifugal loads separately. The maximum strain criterion is applied for each component in the resulting strain and compares it with the allowable values for the local constituent material. Finally, as a mathematical optimization algorithm, a gradient-based constrained optimizer, 'fmincon' command provided in

MATLAB Optimization Toolbox [27] is integrated. This command attempts to find a constrained minimum of a scalar function composed of several variables starting at an initial estimate. This is generally referred to as constrained nonlinear optimization. For a medium-scale optimization problem, 'fmincon' function uses a Sequential Quadratic Programming (SQP) method. Based on that method, the present command solves a Quadratic Programming (QP) sub-problem at each iteration step. An estimate for the Hessian of the Lagrangian is updated at each iteration step using the BFGS [28] formula. Three kinds of termination criteria are provided: the maximum number of iteration, tolerance on the design variables, and tolerance on the function value. When one of these termination criteria is satisfied, the optimization iteration is programmed to be terminated.

Result of Design Optimization for AATR-II Blade

Using the present design optimization framework, it is found that the choice of the initial values for the design variables is quite important, since the design result is sensitive to those selections. Table 4 describes the selected initial values for the present design variables. Figure 7 shows a convergence history of the objective function, i.e., tip twist actuation, for the case the amplitude of input-voltage is limited to 500 V. The design optimization procedure is finished from the termination criteria of the tolerance on the design variables. Throughout design optimization, the maximum tip twist actuation reaches approximately 3.6 ° . In the present result, the magnitude for the amplitude of input-voltage is not important, since a linear relationship between the applied voltage and the twist actuation is established. When an increased input voltage is applied, an increased twist actuation will be obtained. Thus, a goal of the present design optimization is to find an optimal cross-section configuration which produces the maximum twist actuation when a fixed input-voltage is provided.

Figure 8 shows the convergence history of the blade property parameters such as the blade weight, the chordwise-locations of the center of gravity and that of the elastic axis, the first torsional frequency at the nominal rotor speed, and the maximum strain. All the properties of the present AATR-II blade are normalized with respect to those of the original ATR blade, which are in Table 1. Although the AATR-II blade properties become similar to those of the original ATR blade, a few features show up in the process of the AATR-II blade design. As compared with the original ATR blade, the weight of the designed AATR-II blade is very similar. However, the chordwise-locations of the center of gravity and the elastic axis of the AATR-II blade are moved backward slightly. This suggests that the corresponding offsets of the original ATR blade were in front of the quarter chord-line due to an insufficient optimization effort. Furthermore, the first torsion mode frequency at the nominal rotor speed and the maximum strain of the AATR-II blade are slightly lower than the corresponding values of the original ATR blade. It is due to the fact that the present AATR-II blade utilizes a single crystal MFC actuator, which is more flexible than the AFC used in the original ATR blade.

Table 4. Initial values of the design variables for design optimization

Property	Initial value
Starting chordwise-location of active region	0.0455c
Ending chordwise-location of active region	0.65c
Web extension	0.05c
Ballast masses [kg]	(0.15, 0.15)
Ballast mass locations	(0.1c, 0.4c)
Spar location	0.4438c

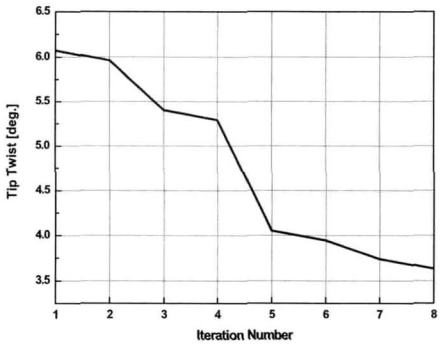

Fig. 7. Convergence history of the objective function: tip twist

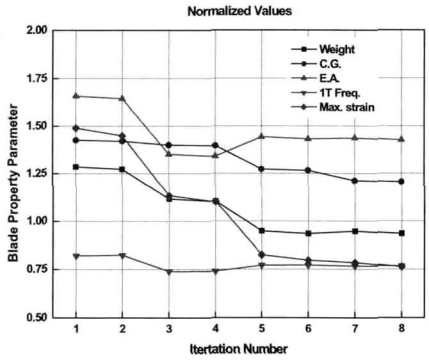

Fig. 8. Convergence history of the blade property parameters

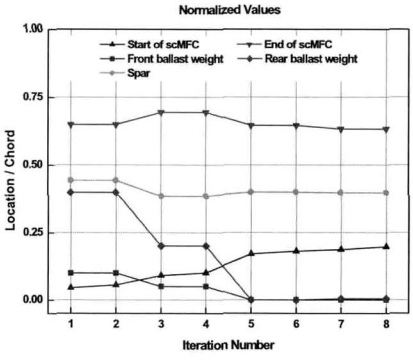

Fig. 9. Convergence history of the blade configuration parameters

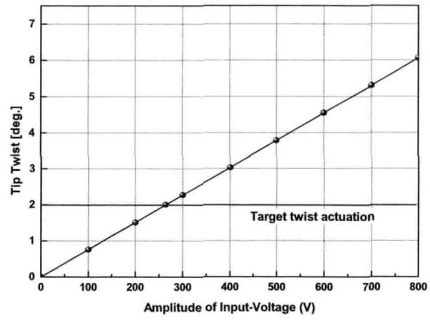

Fig. 10. Minimized input-voltage for target twist actuation

The convergence history of the blade configuration parameters is displayed in Figure 9. For the active region, the starting and ending chordwise-locations are determined to be approximately 19% and 63% of the chord, respectively. The resulting active region length becomes 55% of the allowable active region. Regarding the ballast weights, the rear one moves to the nose, thus all the two ballast weights are located near the nose. This is because the present single crystal MFC actuator, which has a heavier weight density, is distributed from 19% to 63% of the chord. Therefore, the rear ballast weight is not basically required in order to satisfy the center of gravity location at the quarter chord position. The spar of the AATR-II blade is at approximately 40% of the chord, which is moved slightly forward as compared with that of the original ATR blade.

When the design optimization is completed successfully, it is found that the input-voltage in order to achieve the target twist is found to be significantly reduced. Figure 10 shows the relationship between the tip twist actuation and the required input-voltage. As one can see, to obtain the target twist actuation of 2° at the tip, the present cross-sectional configuration requires approximately 264 V. These values correspond to approximately only 13.2% of the input-voltage amplitude required in the original ATR blade. This result suggests that the present AATR-II blade has a capability to reduce the vibration of helicopters with a much lower input-voltage than the original ATR blade does. It is concluded that such an outstanding active-twist performance of the AATR-II blade is achieved through both the use of single crystal MFC actuators and the systematic design optimization effort.

Multi-Body Dynamic Modeling of AATR-II Blade in Forward Flight

In this section, the multi-body dynamic modeling techniques for the AATR-II blade in forward flight condition are discussed. For the multi-body modeling of the AATR-II blade, DYMORE is used in this work. DYMORE is a nonlinear flexible multibody dynamics analysis which has various multi-body element libraries, such as rigid bodies, mechanical joints, and elastic beams. Deformable bodies are modeled with the finite element method. The equations of equilibrium are formulated in a Cartesian inertial frame. Constraints are modeled using the Lagrange multiplier technique. The formulation of beams is based on the geometrically exact beam theory considering the arbitrarily large displacements, finite rotations and small strains [29], but uses the displacement-based form instead of the mixed form. To analyze aerodynamic loads, DYMORE uses finite-state dynamic inflow aerodynamics model [30]. This model is constructed by applying the acceleration potential theory to the rotor aerodynamics problem with a skewed cylindrical wake. More specifically, the induced flow at the rotor disk was expanded in terms of modal functions. As a result, a three-dimensional, unsteady induced-flow aerodynamics model with finite number of states is derived in time domain. This model is an intermediate level of wake representation between the simplest momentum and the most complicate free wake methodologies.

Figure 11 represents the multi-body dynamic modeling of the present four-active-bladed AATR-II system for the forward flight time domain analysis. The hub is modeled as a rigid body, and connected with a revolute joint with a prescribed rotational speed of Ω rad/sec. Root retention is a passive elastic beam attached rigidly to the hub, and the reaction loads at the attachment point are extracted and added over four of them to give the hub vibratory loads. Since the AATR-II hub is fully articulated, three revolute joints are consecutively located between the root retention and the active blade to consider flap, lead-lag, and feathering hinges. A prescribed collective and cyclic pitch control commands are applied at the feathering hinges, and their numerical values are based on those used in the original ATR wind-tunnel experiment. Finally, active beams are attached to represent the AATR-II blades, and they are discretized during the analysis with at least four beam elements per blade, each with the 3rd-order interpolation polynomials. Therefore, there are approximately 900 degrees of freedom to be solved at each time step, including the dynamic inflow state variables for aerodynamics.

Individual Blade Control for AATR-II Blade

For the blade control, in general, there are three available blade control modes including collective twist, differential twist, and Individual Blade Control (IBC). In collective twist control mode, all the blades are under the same synchronous twist actuation signals, while those of an opposite sign are transferred to the blade at the opposite azimuthal location (e.g., Blade No.1 and 3) in differential twist mode. For an IBC actuation mode, the actuation on each blade behaves in the same phase at a specific azimuthal location. Among these control modes, the collective and differential modes were experimentally found to be less effective in reducing the fixed-system vibratory loads when comparing the IBC mode [9]. Therefore, this study adopts the IBC mode using sine-dwell signal with control phase variation. The input-voltage is generated from the following formula:

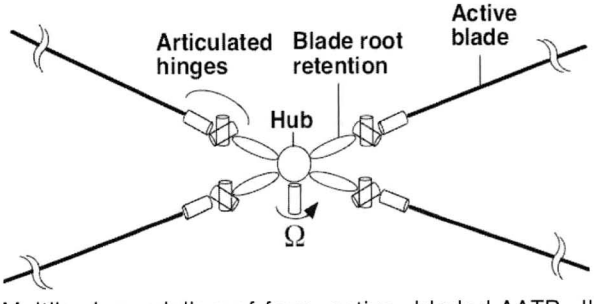

Fig. 11. Multibody modeling of four-active-bladed AATR-II system

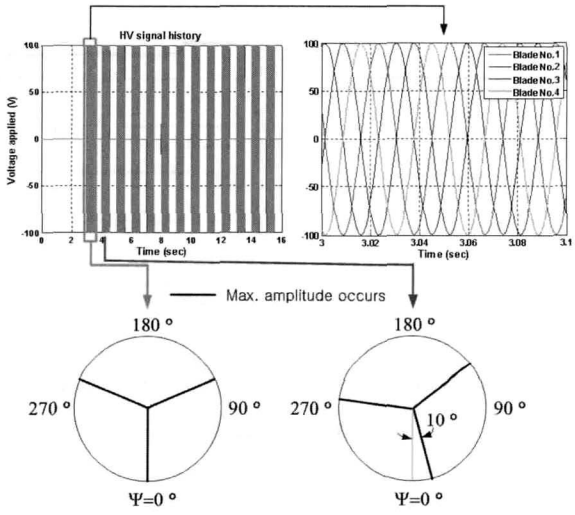

Fig. 12. Example of input-voltage generated for an IBC mode with 3/rev actuation frequency

$$V(t) = V_{\text{amplitude}} \times \cos\left[2\pi\omega_{\text{actuation}}\left(t - \phi_{\text{control phase}}\right) + 2N_{\text{act}}\pi\phi_{\text{blade i}}\right] \tag{3}$$

where

$V_{\text{amplitude}} = 100V$

$\omega_{\text{actuation}} = N_{\text{act}} \times f_{\text{rotation}}$

$\phi_{\text{control phase}} = 0.0, 0.83, ..., 1.0$ (12 divisions over 360 deg.)

$N_{\text{act}} = 3,4,$ or 5

$\phi_{\text{blade i}} = 0.0$ (Blade No.1), 0.25 (Blade No.2), 0.5 (Blade No.3), 0.75 (Blade No.4)

Figure 12 depicts an example of the input-voltage generated for an IBC mode when 3/rev actuation frequency is applied with 12 divisions of the control phase angle. Like the IBC signal of the original ATR blade, there is no actuation for the initial 3 seconds in order to obtain steady-state equilibrium for the forward flight condition. During the last period of this interval, that is, between 2.5 and 3.0s, the baseline loads without actuation on the hub and the blades can be extracted. Then, for each 0.5s period of actuation, each with different control phase angle, and another 0.5s period of no actuation is applied between them. These are applied one after the other as given in Figure 12. Furthermore, by the control phase algorithm as given in Equation (3), the blades have the maximum amplitudes of the sinusoidal electric field at certain azimuthal locations which is shown in Figure 12.

Vibratory Loads Reduction Analysis of AATR-II Blade

In this section, based on the constructed multi-body dynamic modeling for the AATR-II blade, the vibratory loads reduction analysis of the AATR-II blade using the present cross-sectional configuration from the design optimization is conducted. Through the vibratory loads prediction for the fixed- and rotating-system, it will be shown that the AATR-II blade may reduce the vibration of rotorcrafts more efficiently when comparing the previous ATR blades. As mentioned in the previous section, the amplitude of input-voltage to the AATR-II blade is assumed to be 100 V. This value corresponds to only 10% input-voltage of the original ATR blade using AFC actuators.

The forward flight condition is considered as the advance ratio $\mu = 0.140$, the rotor shaft angle of attack $\alpha_s = -1°$ and the non-dimensional thrust coefficient $C_T = 0.0066$. For the trim under this forward flight condition, target thrust is chosen as 1000 N, and target

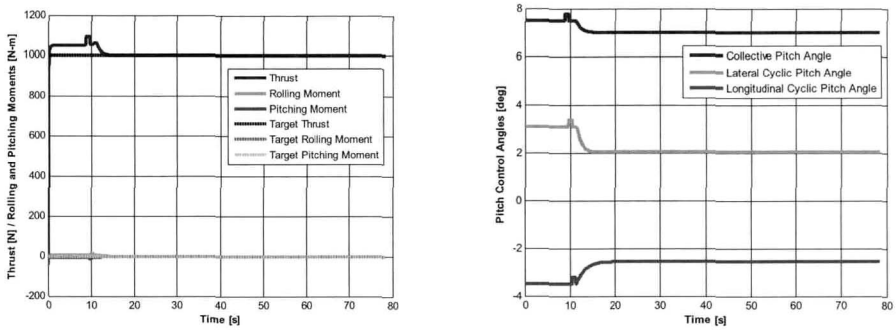

(a) Trimmed thrust and rolling/pitching moments (b) Trimmed pitch control angles

Fig. 13. Trim analysis results of AATR-II

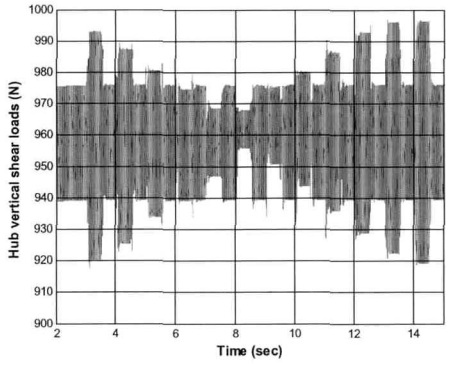

Fig. 14. Time history of hub vertical shear loads with 3/rev actuation frequency

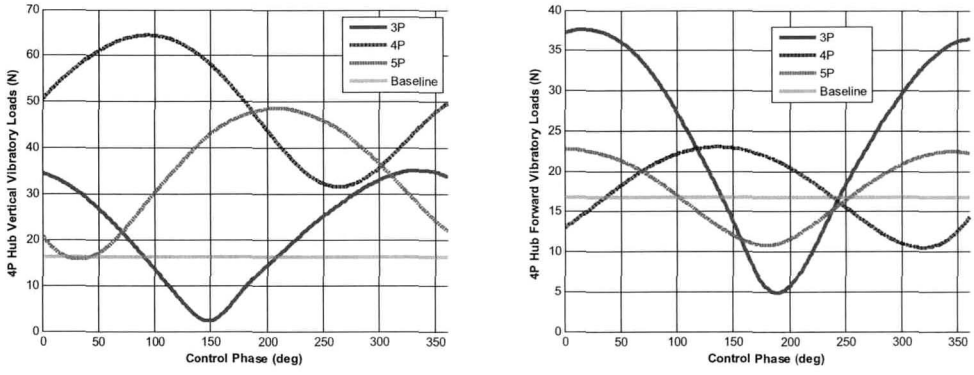

(a) Vertical component (b) Forward component

Fig. 15. Variation of 4/rev hub shear vibratory loads

rolling/pitching moments are selected as both 0 N-m. Figure 13 gives the result of trim analysis for AATR-II. As one can see, all three values of thrust, rolling and pitching moments are converged well to the target values. In addition, the trimmed pitch control angles for collective and two cyclic controls are obtained.

After the trim analysis is completed, first the vibratory loads at the hub are predicted. The hub loads of the rotor system can be obtained from summation of all the loads in the four root retention elements at the root. Figure 14 shows the time history of hub vertical shear forces when the 3/rev actuation frequency is applied. As one can see the vibratory

loads magnitude is changed considerably for certain control phase actuation. The biggest reduction is observed for 8 to 8.5s. Through conversion from time domain results to frequency domain, the 4/rev hub shear vibratory load component is predicted since the 4/rev loads component is the most dominant component for the four-bladed rotor system.

Figure 15 gives the variation of the 4/rev hub shear vibratory loads when the 3, 4, and 5/rev actuation frequency is applied with the control phase. As one can see, the hub vertical shear load component is reduced by approximately 86% when the 3/rev actuation frequency with 149° control phase is applied. This reduction result of the AATR-II blade is comparable with that of the original ATR blade, although only 10% input-voltage of the original ATR blade is applied to the AATR-II blade. For the hub forward shear load component, the 3/rev actuation frequency is also the most effective when 190° control phase is considered and it can reduce the hub forward shear load component by 71%.

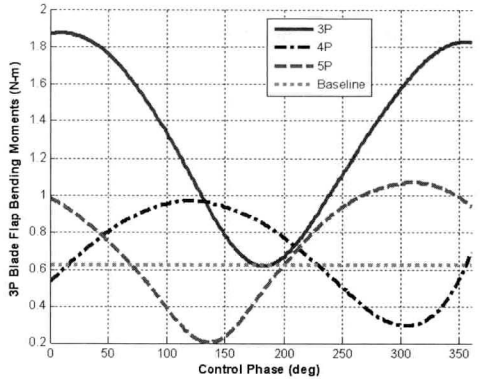

(a) 3/rev component

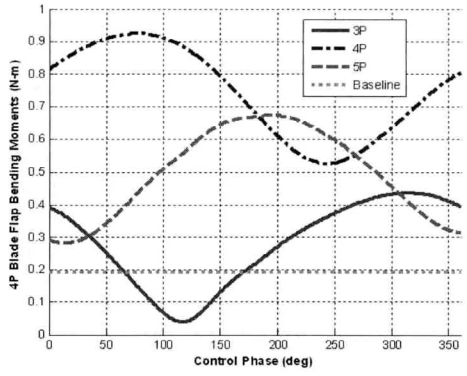

(b) 4/rev component

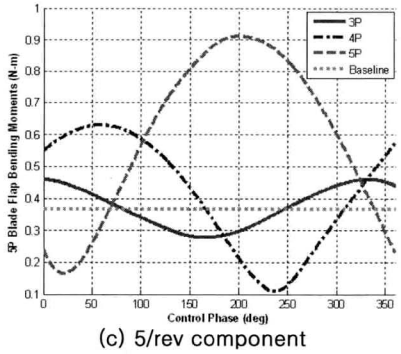

(c) 5/rev component

Fig. 16. Variation of blade flap bending moment at 28.7% span location

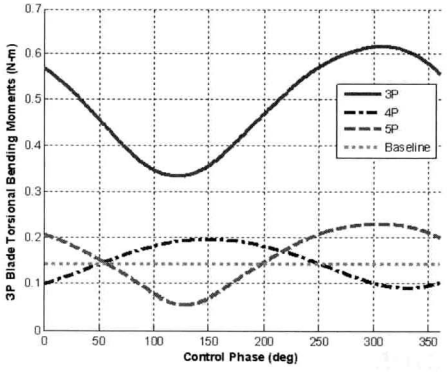

(a) 3/rev component

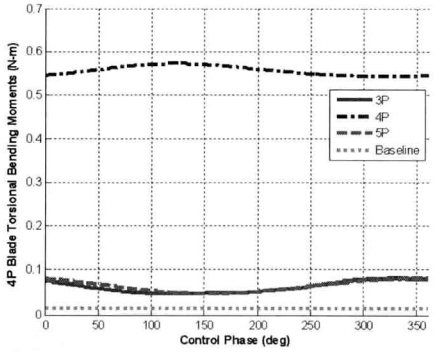

(b) 4/rev component

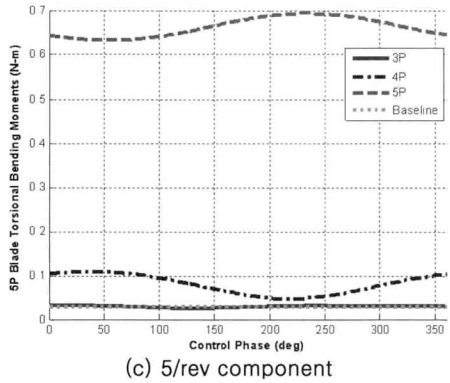

(c) 5/rev component

Fig. 17. Variation of blade torsional moment at 33.6% span location

Following the prediction for the vibratory loads at the hub, the rotating-system loads such as the flap bending moment and the torsional moment of the blade are predicted. Unlike the previous fixed-system loads, there are the 3, 4, and 5/rev frequency load components in the rotating-system loads. The 3, 4, and 5/rev frequency load components of the flap bending moment at 28.7% span location are shown in Figure 16. As one can see, for all frequency load components, the flap bending moments can be reduced significantly. Figure 17 shows the 3, 4, and 5/rev frequency load components of the torsional moment at 33.6% span location. On the contrary to the previous results, the torsional moments are increased significantly. The N/rev actuation frequency (N=3, 4, and 5) increases the N/rev frequency torsional moment, respectively. This is due to the active twisting actuation. Therefore, a special attention is required since it may degrade the blade fatigue life. In the future, a more advanced design optimization framework which includes an aeroelastic analysis at each design step will be constructed. This problem will be considered as one of its design requirements and the solution will be provided. Through the present vibratory loads reduction analysis results of the AATR-II blade in forward flight, it is shown that the AATR-II reduces the vibratory loads on the fixed- and rotating-systems significantly even with a much lower electric power consumption. This is due to that both the outstanding piezoelectric strain constants of the single crystal MFC and the systematic design optimization allow the present AATR-II blade to have an excellent performance and efficiency in reducing the vibratory loads of rotorcrafts.

Although the present numerical results reveal that the AATR-II blade incorporating single crystal MFC has an improved capability to reduce the vibratory loads in helicopters, there are still two major obstacles for single crystal piezoelectric fiber composites regarding application to a full scale helicopter rotor. One of those is severe brittleness of the single crystal piezoelectric material. As mentioned in previous section, since there is not available value for maximum allowable strain of it, that corresponding to the standard MFC is used instead. However it is well known that the single crystal piezoelectric material is more brittle than the conventional piezoelectric material. Although the combination of single crystal piezoelectric fibers and epoxy matrix may improve the strength characteristics of the composite actuator, it still exhibits a lower value than that for the standard piezoelectric fiber composites. This drawback may be relieved by reinforcing the single crystal piezoelectric fiber composites with additional glass fibers while they are fabricated. Second is the difficulty of the single crystal piezoelectric material in manufacturing in a large size. This problem is expected to be solved by a rapid development in its fabrication technique.

Conclusion

This paper proposes a brand new integrally twist-actuated blade utilizing single

crystal piezoelectric fiber composites. It also conducts its aeroelastic analysis in forward flight. In order to design the new AATR-II blade, a design optimization established previously for an active helicopter blade is further improved and used. The present design optimization framework consists of the 2-D cross-sectional analysis, the 1-D beam analysis, the gradient-based optimizer and various related modules. The AATR-II blade is designed to maintain the blade properties of the original ATR blade. After the design optimization of the AATR-II blade is completed successfully, the vibratory loads reduction analysis of the present AATR-II blade in forward flight condition is conducted by using the multibody modeling for the AATR-II blade. With only 10% input-voltage of the original ATR blade applied to the AATR-II blade, it reduces the vibratory loads on the fixed- and rotating-system by a similar level as that capable in the original ATR. The numerical results show that the AATR-II blade can reduce the vibratory loads of the helicopter more efficiently when comparing the previous ATR blade. However, in order to manufacture the present ATR blade using single crystal piezoelectric fiber composites and for its application to a full scale rotorcraft, it is needed to pay attention to drawbacks of the single crystal piezoelectric materials, such as a difficulty in manufacturing in a large size and a very brittle characteristic. A further investigation considering such issues will be conducted for the realistic blade design and analysis.

Acknowledgement

This work is supported by the Korean Aerospace Research Institute under Korean Helicopter Project Dual-Use Component Development Program funded by the Ministry of Commerce, Industry, and Energy. It is also supported by Grant No. R01-2006-000-10059-0 from the Basic Research Program of the Korea Science and Engineering Foundation. The authors would like to express their acknowledgment to Dr. O. A. Bauchau of the Georgia Institute of Technology for providing access to the analysis code DYMORE; and also to Dr. C. E. S. Cesnik and Ms. J. Mok of the University of Michigan for providing access to the design optimization framework and their helpful discussions.

References

1. Shaw, J., Albion, N., Hanker, E. J., and Teal, R. S., "Higher Harmonic Control: Wind Tunnel Demonstration of Fully Effective Vibratory Hub Force Suppression", Journal of the American Helicopter Society, Vol. 31, No. 1, 1989, pp. 14-25.

2. Ham, N. D., "Helicopter Individual-Blade-Control Research at MIT 1977-1985", Vertica Vol. 11, No. 1/2, 1987, pp.109-122.

3. Ham, N. D., "Helicopter Individual-Blade-Control Research at MIT 1977-1985", Vertica Vol. 11, No. 1/2, 1987, pp.109-122.

4. Wood, E. R., Power, R. W., Cline, J. H., and Hammond, C. E., "On Developing and Flight Testing a Higher Harmonic Control System", Journal of the American Helicopter Society Vol. 30, No. 2, 1985, pp. 3-20.

5. Bent, A. A., "Active Fiber Composites for Structural Actuation", PhD Thesis, Department of Aeronautics and Astronautics, Massachusetts Institute of Technology, 1997.

6. Wilkie, W. K., Bryant, R. G., High, J. W., Fox, R. L., Hellbaum, R. F., Jalink, A. Jr., Little, B. D., and Mirick, P. H., "Low-Cost Piezocomposite Actuator for Structural Control Applications", Proceedings of SPIE 7th Annual International Symposium on Smart Structures and Materials, Newport Beach, CA, 2000.

7. Wilbur, M., L., Yeager, Jr. W. T., Wilkie, W. K., Cesnik, C. E. S., and Shin. S. -J., "Hover Testing of the NASA/ARMY/MIT Active Twist Rotor Prototype Blade", Proceedings of the American Helicopter Society 56th Annual Forum, Virginia Beach, VA, 2000.

8. Cesnik, C. E. S., and Shin, S. -J., and Wilbur, M. L., "Dynamic Response of Active Twist Rotor Blades", Smart Materials and Structures-Special Issue on Rotorcraft Applications, Vol.10, No.1, 2001, pp. 62-76.

9. Wilbur, M. L., Mirick, P. H., Yeager, Jr. W. T., Langston, C. W., Cesnik, C. E. S., and

Shin, S. -J., "Vibratory Loads Reduction Testing of the NASA/Army/MIT Active Twist Rotor", Journal of the American Helicopter Society, Vol.47, No.2, 2002, pp.123-133.

10. Wilbur, M. L., Yeager, Jr. W. T., and Sekula, M. K., "Further Examination of the Vibratory Loads Reduction Results form the NASA/Army/MIT Active Twist Rotor Test", Proceedings of the American Helicopter Society 58th Annual Forum, Montreal, Canada, 2002.

11. Shin, S. -J., and Cesnik, C. E. S., and Hall, S. R., "Closed-Loop Control Test of the NASA/Army/MIT Active Twist Rotor for Vibration Reduction", Proceedings of the American Helicopter Society 59th Annual Forum, Phoenix, AZ, 2003.

12. Sekula, M. K., Wilbur, M. L., and Yeager, Jr. W. T., "Aerodynamic Design Study of an Advanced Active Twist Rotor", Proceedings of the American Helicopter Society 4th Decennial Specialist' s Conference on Aeromechanics, San Francisco, CA, 2004.

13. Masarati, P., Morandini, M., Riemenscheider, J., Wierach, P., Barkanov, E., and Gluhih, S., "Optimal Design of an Active Twist 1:2.5 Scale Rotor Blade", Proceedings of 31st European Rotorcraft Forum, Florence, Italy, 2005.

14. Wierach, P., Riemenscheider, J., and Keye, S., "Development of an Active Twist Rotor Blade with Distributed Actuation and Orthotropic Material", Proceedings of SPIE: Smart Structures and Integrated Systems, San Diego, CA, 2005.

15. Li, T., Scotch, A. M., Chan, H. M., Harmer, M. P., Park, S. -E., Shrout, T. R., and Michael, S. J., "Single Crystals of $Pb(Mg_{1/3}Nb_{2/3})O_3$-35 mol% $PbTiO_3$ from Polycrystalline Precursors", Journal of American Ceramic Society, Vol. 81, No.1, 1998, pp. 244-248.

16. Wilkie, W. K., Inman, D. J., and Lloyd, J. M., "Anisotropic Laminar Piezocomposite Actuator Incorporating Machined PMN-PT Single Crystal Fibers", Journal of Intelligent material systems and structures, Vol.17, No. 11, 2006, pp. 15-28.

17. Park, J. -S., and Kim, J. -H., "Analytical Development of Single Crystal Macro Fiber Composite Actuators for Active Twist Rotor Blades", Smart Materials and Structures, No.14, No.4, 2005, pp. 745-753.

18. TRS Ceramics, Inc. http://www.trsceramics.com

19. Chattopadhyay, A., Seeley, C. E., and Mitchell, "Design of a Smart Flap Using Polymeric C-Block Actuators and a Hybrid Optimization Technique", Smart Materials and Structures, Vol. 6, No.2, 1997, pp. 134-144.

20. Sahasrabudhe, V., Chen, P. C., Thompson, P. M., and Aponso, B. L., "Integrated Design of Smart Rotor and Robust Control System", Proceedings of SPIE: Smart Structures and Integrated Systems, San Diego, CA, 1998.

21. Zang, J., Smith, E. C., and Wang, K. W., "Active-Passive Hybrid Optimization of Rotor Blades with Trailing Edge Flaps", Journal of the American Helicopter Society, Vol. 49, No.1, 2004, pp. 54-65.

22. Cesnik, C. E. S., Mok, J. -W., Parikh, A. S., and Shin, S. -J., "Optimization Design Framework for Integrally Twisted Helicopter Blades", Proceedings of 45th AIAA/ASME/ASCE/AHS/ASC Structures, Structural Dynamics and Materials Conference, Palm Springs, CA, 2004.

23. Cesnik, C. E. S., Mok, J. -W., Morillo, J. A., and Parikh, A., "Design Optimization of Active Twist Rotor Blades", Proceedings of 30th European Rotorcraft Forum, Marseilles, France, 2004.

24. Bauchau, O. A., "Computational Schemes for Flexible, Nonlinear Multi-Body Systems Multibody System Dynamics", Vol. 2, 1998, pp. 169-225.

25. Cesnik, C. E. S., and Palacios, R., "Modeling Piezocomposite Actuators Embedded in Slender Structures", Proceedings of 44th AIAA/ASME/ASCE/AHS/ASC Structures, Structural Dynamics and Materials Conference, Norfolk, VA, 2003.

26. Brown, E. L., "Integrated Strain Actuation in Aircraft with Highly Flexible Composite Wings", PhD Thesis, Department of Aeronautics and Astronautics, Massachusetts Institute of Technology, 2003.

27. Coleman, T. F., and Zhang, Y., "Optimization Toolbox for Use with MATLAB", The MathWorks Inc., 1999.

28. Rao, S. S., "Engineering Optimization: Theory and Practice," John Wiley & Sons, Inc., 1996.

29. Hodges, D. H., "A mixed variational formulation based on exact intrinsic equations for dynamics of moving beams", International Journal of Solids and Structures, Vol. 26, No.11, 1990, pp.1253-73.

30. Peters, D. A., and He, C. J., "Finite State Induced Flow Models Part II: Three Dimensional Rotor Disk", Journal of Aircraft, Vol. 32, No 2, 1995, pp. 323-333.

List of Tables and Figures

List of Tables

List of Figures